Determination of low latitude electric fields from FUV images

Thomas J. Immel, Stephen B. Mende, Harald U. Frey, Laura M. Peticolas

Space Sciences Laboratory, University of California, Berkeley

Eiichi Sagawa

Communications Research Laboratory, Tokyo, Japan

Abstract.
Thousands of images of the nighttime equatorial airglow arcs have been obtained by the far-ultraviolet imager (FUV) on-board the NASA IMAGE satellite. Imaging periods lasting several hours around the time of satellite apogee allow for the determination of the velocity of drifting plasma density depletions occurring within the airglow arcs. These velocities reflect the ExB drift of low-latitude plasma under the influence of a vertical electric field. A survey of several weeks of data produces information regarding the range of electric field magnitudes, and the spatial and temporal frequency of the appearance of plasma depletions. It is found that plasma depletions are observed during >80% of the successive 4-6 hour imaging periods, with significant absences during periods of high magnetic activity. Furthermore, comparisons between |E| and solar 10.7-cm radio flux shows evidence of the direct effect of solar output on nightside electric fields.

1. Introduction

The terrestrial equatorial airglow arcs, like the auroral ovals, are persistent features of Earth's far-ultraviolet (FUV) signature [*Carruthers and Page*, 1976]. The arcs appear as a pair of emission bands on either side of Earth's magnetic equator, extending from the dusk terminator eastward across the nightside. Unlike the aurora, their intensity does not indicate the strength or rate of coupling to the magnetosphere, but rather the state of the equatorial ionosphere [*Sojka*, 1991]. The arcs indicate regions of enhanced ionospheric densities where ionospheric plasma is concentrated after rising from the magnetic equator under the influence of daytime dynamo electric fields. The concentration occurs as the plasma diffuses along magnetic field lines which, to the north and south of the magnetic equator, direct the plasma downward into regions of higher plasma densities [*Hanson and Moffett*, 1966]. Due to the complex interaction of the ionosphere and thermosphere in the low-latitude evening sector, localized instabilities can rapidly grow in altitude, resulting in strong localized depletions in plasma densities, with corresponding decreases in airglow brightness in the airglow arcs [*Weber et al.*, 1978]. From years of observations by radars based at low latitudes come the terms "spread-F" to describe the conditions of the destabilized F-region, and "bubbles" or "plumes" to describe the ionospheric depletion associated with the fully developed spatial instability, which is the cause of the large-scale airglow depletions [*Kelley*, 1989].

New global scale studies of these phenomena are now possible using the spectrographic imaging component of the Far Ultraviolet Imager on the IMAGE satellite [*Burch*, 2000; *Mende et al.*, 2000a]. In this study the SI-13 channel is used, which, with its 5-nm passband centered at 135.6 nm, is specifically designed for observations of that emission of atomic oxygen [*Mende et al.*, 2000b]. For auroral or dayside studies, care must be taken to interpret the images with the knowledge that particular emissions of the Lyman Birge Hopfield bands of N_2 also lie in the imager's passband. Since the molecular emission is only produced by direct impact of ~10 eV electrons on N_2, either photoelectrons or sec-

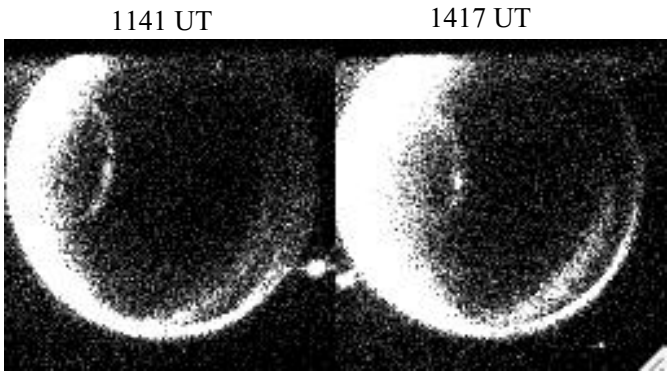

Figure 1. A pair of 135.6-nm images of Earth obtained by the SI-13 instrument on March 28, 2002 (day 87) at 1141 and 1417 UT.

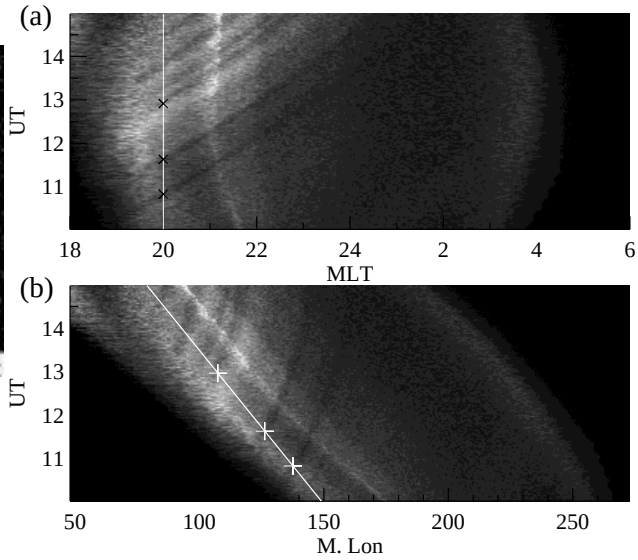

Figure 2. Magnetic Local Time and Longitude keograms of Day 87, 2002, SI-13 imaging period. (a) MLT-UT keogram, showing advance of 135.6-nm O I brightness depressions in local time. (b) Mag. Longitude-UT keogram, showing advance of brightness depressions in magnetic longitude. In each plot the 20 MLT location is indicated with a solid line, on which the crossing times of 3 significant depletions is marked.

ondary auroral electrons, it does not contribute to the SI-13 signal during observations of low latitudes on the nightside.

2. IMAGE Observations

The IMAGE satellite was placed in a highly elliptical orbit (perigee altitude=1000 km, apogee altitude=7.2 R_E) in March of 2000. Apsidal motion of the orbit has caused the latitude of apogee to proceed from 40° to 90° and back down to cross the equator in early 2003. In March, 2002, the latitude was sufficiently low to consistently view the northern airglow arc, with improved viewing of the southern anomaly by May. It is during these months when the local time of apogee is in the evening sector, providing a clear view of the airglow arc from the evening terminator to post-midnight local times. The FUV imaging cadence matches the rotation rate of the satellite which is 2 minutes, with 5 seconds of integration time per SI-13 image.

Two imaging examples are provided in Figure 1, obtained at 1141 and 1417 UT on Day 87 (March 28), 2002. Though the latitude of the satellite moves from 53.7° to 64.9°, the northern airglow arc remains visible. Furthermore, the arc brightens over the time period, with brightnesses > 300 Rayleigh (R) extending to the midnight sector and over a broader range of magnetic latitude. The conversion to brightness from instrument counts is performed according to the UV stellar calibration of the instrument described by *Frey et al.* [2003].

3. Analysis Technique.

Full time series of images must be examined to determine the development of spatial and temporal variations in the arc's brightness. To do this, the images are re-mapped to a regularly spaced grid of magnetic local time (MLT) and latitude (Mag. Lat.), and the instrument counts between 0 and 30° Mag. Lat. are added to report a single number for each 0.5° increment of MLT [see also *Sagawa et al.*, 2003, for further use of this technique]. Processing all available images for an imaging pass results in a data set which can be presented as a keogram, with UT on the vertical axis and MLT on the horizontal axis. The keogram reveals the relative MLT motion of brightness irregularities as a function of UT. For this and all further work, the APEX magnetic coordinate system is used [*Richmond*, 1995].

The MLT-UT keogram for the imaging period including the images of Figure 1 is shown in Figure 2a. The decreases in total 135.6-nm emission intensity in the airglow arc is revealed in this presentation by the several dark tracks which advance in MLT as a function of UT. These are not imaging artifacts, as any such problem (e.g. incorrect flat-fielding) would not move rapidly in local time. Indeed, the flatfield for this imaging period is imperfect, and the bright stripe which is localized between 21 and 22 MLT is an artifact of the incorrect flatfield. This does not interfere with the continued analysis of the O I brightness depressions, and it demonstrates

the significant difference between the signature of O I brightness depressions and imaging artifacts.

The apparent motion of the brightness decreases in MLT is obvious, and the keogram clearly shows the development of 5 patches which cross the MLT=20 hours sector at 1050, 1140, 1255, 1310, and 1340 UT. There is also a traveling enhancement in brightness which crosses MLT=20 around 1230. In terms of development of spread-F in the evening sector, this is an active period with instabilities growing into multiple large plumes in < 4 hours time.

An approach which identifies the motion of the brightness decreases with respect to positions fixed on Earth is developed and shown in Figure 2b for the same imaging period. In this presentation, the horizontal axis shows the magnetic longitude (Mag. Lon.) of the FUV measurements during the same time period as in Figure 2a. Features fixed with respect to the ground will appear as vertical traces in this display. For reference, the 20 MLT position is indicated with a solid line, decreasing in latitude with time. The FUV brightness decreases are again obvious in this presentation and clearly demonstrate a drift toward greater longitudes (eastward). What is also clear from the pair of plots in Figure 2 is that the drifts are most rapid at early evening local times, slowing down by a factor of 2 or more by midnight. The first three depletions to pass through the 20 MLT sector are indicated in each panel of Figure 2 and will be further analyzed in this report.

To determine the drift speed of individual plasma depletions, the Mag. Lon. and UT of the center of the depletion is determined at 15 points in the keogram, and a least-squares fit to the data is determined, using a 4-th degree polynomial. The derivative of the fitted data is then calculated, giving the fitted instantaneous velocity of the drifting depletion over the time of observation. This method is applied for 3 separate depletions and the results shown in Figure 3. The three depletions are those crossing the 20 MLT sector at 1050, 1140 and 1255 UT. Plotted now with UT on the abscissa, the position as a function of time for the 3 depletions is shown in Figure 3a, with the polynomial fits overlaid. The derivatives of the 3 fits are shown in Figure 3b, which show the instantaneous drift speed as a function of MLT. The speeds are greatest in early evening, with values between 8 and 12 degrees/hour, or 50-80% of corotational velocities, in the 20 MLT sector, where the values are highlighted with asterisks.

This technique is applied to each imaging set from days 87-129, 2002, and the resulting drift speeds in the 20 MLT sector are shown in Figure 4 for each plasma

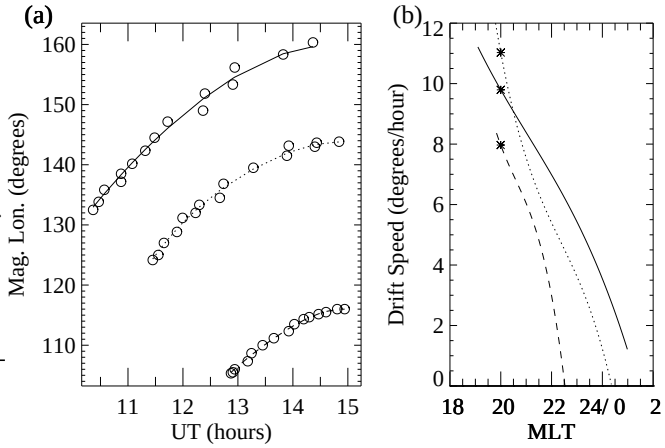

Figure 3. Drift data fitted to determine drift velocity (a) The track of three of the brightness decreases from Figure 2b in UT vs. Mag. Lon., with 4-th degree polynomial fits overlaid. (b) Speed of the brightness depletions in degrees per hour. Solid, dotted, and dashed lines are used to separately indicate each of the three traces from Figure 3a. The speeds at 20 MLT, highlighted in Figure 4, are highlighted with asterisks.

depletion observed in the keograms. The three drift speeds determined in Figure 3b are encircled. The drift speeds in this MLT sector show a definite decreasing trend over time. In searching for an explanation for this, variation in magnetic activity is ruled out, as the Kp indices show equally low levels of activity before and after the day 107-110 storm period. And though there is a known seasonal effect with greater drift speeds during equinox, the spring-summer seasonal variability is expected to be less significant than the observed decrease [*Fejer*, 1993], which occurs over only a month of time.

A significant change in solar radio flux ($F_{10.7}$) occurred during the >40 day imaging period, mainly decreasing over time as well. The values of $F_{10.7}$ are shown in Figure 4 with a solid line. The solar radio flux is known to correspond well with solar EUV output on time scales of days and longer [*Hedin*, 1984], and its correspondence with nightside drift speed is striking. This correspondence most likely lies in the physical coupling between dayside heating/ionization, and nightside neutral wind speeds/vertical electric field strength, and reflects the increase in nightside neutral winds under intensified solar EUV output [*Biondi et al.*, 1999].

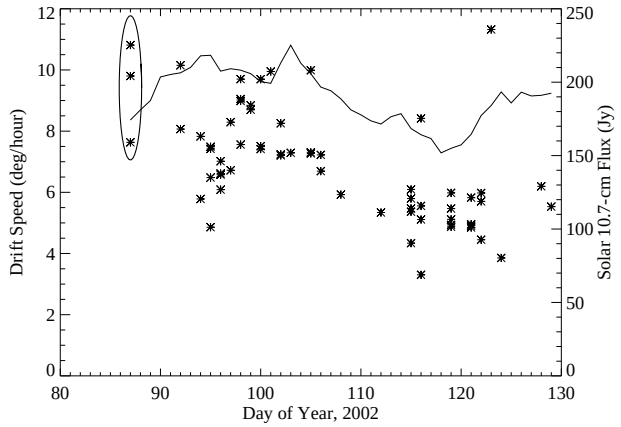

Figure 4. Plasma drift velocities at 20 MLT for >40 days in 2002. The eastward velocity of identifiable plasma depletions is determined as shown in Figure 3 for every IMAGE observational period between days 82 and 129, 2002. The instantaneous velocity at 20 MLT is shown from each day with an asterisk. The solid plotted line indicated the solar 10.7-cm radio flux, on a scale indicated by the right axis. Values determined in Figure 3b are encircled.

4. Discussion

Assuming the magnetic equator is a great circle about the planet, the zonal plasma drift speeds are $230< v_i <350$ m/sec in the 20 MLT sector between 11 and 14 UT on day 87, corresponding to rather strong vertical electric fields in the 6-8.5 mV/m range. The average electric field in this sector (from Figure 4) is found to be 5.0 mV/m, dropping to 3.0 mV/m at midnight (not shown). These values are somewhat larger than what may be expected from earlier studies, though the local time variation is consistent [*Fejer*, 1993]. At this point the true ground speed of the drifting patches is not calculated or shown, and transformation to an orthogonal coordinate system must be done for exact determination of drift speeds and electric fields.

The range of the vertical electric field in the 20 MLT sector is determined by the use of a least squares fit to the average daily electric field as a function of $F_{10.7}$. The range of $F_{10.7}$ values is 152-225 Jy, corresponding to a range of electric fields of 5.6-8.2 mV/m. The increases in $F_{10.7}$ and $E_{Vertical}$ are 48% and 45%, respectively, showing a very good correspondence of the two parameters.

The frequency of significant plasma depletions can be roughly estimated from the traces obtained from measurable depletions during the study period (71 traces in 182 hours). This includes nightside observation times where no plasma depletions were observed, so the occurrence rate for depletions is found to be on the order of one per 2.5 hours. The rate can be much higher, with periods of nearly two per hour observed. On the other hand, the rate is much lower during the April 7-10, 2002 magnetic storm, during which few drifting density depletions are observed.

5. Conclusion

This paper describes the first space-based FUV observations of drifting low-latitude plasma depletions. Assuming the drifting depletions are embedded in the ionospheric plasma, the drift speed can be determined, and the vertical electric field calculated. The drift speeds are also indicative of the zonal neutral wind velocities which, at low latitudes on the nightside, are generally equal to the eastward plasma drift velocity [*Valladares et al.*, 2002]. The modulation of the nightside velocities in apparent response to solar EUV output is a self-consistent effect produced by increased solar heating on the dayside, which drives stronger F-region neutral winds, and increases F-region ionospheric densities globally, which combine to enhance the nightside vertical electric fields. These results will be compared to new observations of the airglow arcs obtained in early 2003 to better determine whether the variation in solar output is truly the driver for the nightside drift speed variation.

Further observations in 2003, including direct conjugate observations of the southern arc, will be useful in addressing the question of plasma bubble frequency vs. magnetic activity. Also, the degree of conjugacy of the arcs during equinox conditions will be important for discussions of high-latitude effects on the equatorial ionosphere. Observation of the development of plasma density decreases associated with spread-F and the simultaneous determination of plasma drift speeds across the active evening ionosphere could prove to be a very significant contribution to the mature field of equatorial ionospheric physics.

Acknowledgments. IMAGE FUV analysis is supported by NASA through Southwest Research Institute subcontract number 83820 at the University of California, Berkeley, contract NAS5-96020.

References

Biondi, M. A., S. Y. Sazykin, B. G. Fejer, J. W. Meriwether, and C. G. Fesen, Equatorial and low latitude thermospheric winds: measured quiet time variations with season and solar flux from 1980 to 1990, *J. Geophys. Res.*, *104*, 17,091–17,106, 1999.

Burch, J. L., IMAGE mission overview, *Space Sci. Rev.*, *91*, 1–14, 2000.

Carruthers, G. R., and T. Page, Apollo 16 far ultraviolet imagery of the polar auroras, tropical airglow belts, and general airglow, *J. Geophys. Res.*, *81*, 483–496, 1976.

Fejer, B. G., F Region plasma drifts over Arecibo:Solar cycle, seasonal and magnetic activity effects, *J. Geophys. Res.*, *98*, 13,645–13,652, 1993.

Frey, H. U., et al., Summary of quantitative interpretation of IMAGE far ultraviolet auroral data, *Space Sci. Rev.*, p. in press, 2003.

Hanson, W. B., and R. J. Moffett, Ionization transport effects in the equatorial F region, *J. Geophys. Res.*, *71*, 5559, 1966.

Hedin, A. E., Correlations between thermospheric density and temperature, solar EUV flux, and 10.7-cm flux variations, *J. Geophys. Res.*, *89*, 9828–9834, 1984.

Kelley, M. C., *The Earth's Ionosphere Plasma Physics and Electrodynamics*, Academic Press, Inc., San Diego, 1989.

Mende, S. B., et al., Far ultraviolet imaging from the IMAGE spacecraft. 1. Systems design, *Space Sci. Rev.*, *91*, 243–270, 2000a.

Mende, S. B., et al., Far ultraviolet imaging from the IMAGE spacecraft. 3. Spectral imaging of Lyman-α and OI 135.6 nm, *Space Sci. Rev.*, *91*, 287–318, 2000b.

Richmond, A. D., Ionospheric electrodynamics using magnetic apex coordinates, *J. Geomagn. Geoelectr.*, *47*, 191–212, 1995.

Sagawa, E., T. Maruyama, T. J. Immel, H. U. Frey, and S. B. Mende, Global view of the nighttime low latitude ionosphere by the 135.6 nm OI observation with IMAGE/FUV, *Geophys. Res. Lett.*, p. submitted, 2003.

Sojka, J. J., Ionospheric physics, *Rev. Geophys.*, *29*, 1166–1186, 1991.

Valladares, C. E., J. W. Meriwether, R. Sheehan, and M. A. Biondi, Correlative study of neutral winds and scintillation drifts measured near the magnetic equator, *J. Geophys. Res.*, *107*, 10.1029/2001JA000,042, 2002.

Weber, E. J., J. Buchau, R. H. Eather, and S. B. Mende, North-south aligned equatorial airglow depletions, *J. Geophys. Res.*, *83*, 712–716, 1978.

T. J. Immel, S. B. Mende, H. U. Frey, L. M. Peticolas, Space Sciences Laboratory, University of California, Berkeley, CA, 94720 (email: immel@ssl.berkeley.edu)

Eiichi Sagawa, Communications Research Laboratory, Tokyo, Japan (email:esagawa@crl.go.jp)

Received February 27, 2003; accepted ? ?, 2003.

This preprint was prepared with AGU's LaTeX macros v5.01, with the extension package 'AGU^{++}' by P. W. Daly, version 1.6b from 1999/08/19.